Electronic Compressibility of a Graphene Bilayer

S. Viola Kusminskiy, Johan Nilsson, D. K. Campbell, and A. H. Castro Neto

Department of Physics, Boston University, 590 Commonwealth Ave., Boston, Massachusetts 02215, USA

(Received 28 June 2007; published 12 March 2008)

We calculate the electronic compressibility arising from electron-electron interactions for a graphene bilayer within the Hartree-Fock approximation. We show that, due to the chiral nature of the particles in this system, the compressibility is rather different from those of either the two-dimensional electron gas or ordinary semiconductors. We find that an inherent competition between the contributions coming from intraband exchange interactions (dominant at low densities) and interband interactions (dominant at moderate densities) leads to a nonmonotonic behavior of the compressibility as a function of carrier density.

DOI: 10.1103/PhysRevLett.100.106805 PACS numbers: 81.05.Uw, 51.35.+a

The recently developed experimental capability of isolating and manipulating an arbitrary number of graphene layers [1] has attracted considerable attention both for its impact on basic science [2] and for the tantalizing potential technological applications. The graphene bilayer is particularly interesting because of the possibility of opening—and controlling—a gap in the electronic spectrum by applying an external electric field [3–6]. This is not possible for the single layer graphene. The bilayer, therefore, while inheriting many of the peculiar electronic characteristics of the monolayer due to its chiral Dirac fermion (though massive) spectrum, has the added virtue of being capable of acting as an electronic switch. It is thus essential to obtain a comprehensive characterization of this material. While some transport experiments are available [7], thermodynamic measurements are largely lacking. Among the thermodynamic quantities to be measured, the electronic compressibility κ stands out as an excellent tool to provide insight into the many-body interactions present in this material. κ can be obtained from the ground state energy as

$$\kappa^{-1} = n_e^2(\partial^2 E/\partial n_e^2), \tag{1}$$

where E is the ground state energy per unit area, and n_e is the electronic density. The electronic compressibility of a single layer graphene has been recently measured [8], and its behavior, besides being remarkably different from that of the usual two-dimensional gas (2DEG), seems to indicate that contributions from Coulomb interactions are either very weak or cancel out. Hartree-Fock [9] and Random Phase Approximation (RPA) [10] calculations predict a correction between 10 and 20% to the free theory for experimentally realized dopings. This correction increases logarithmically as the doping is lowered. It is natural then to ask what role interactions play in the bilayer. In many aspects, the bilayer graphene closely resembles the 2DEG, as described below. Hence, the bilayer system provides an opportunity to isolate the effects arising from its single layer constituents, from those occurring in an ordinary 2DEG. In particular, the issue of the chirality, which is so important for weak-localization physics [11], is the main difference between these two systems, and as we will show, plays an important role in the many-body physics of the bilayer. For small doping, the bilayer can be mapped approximately to a chiral two-dimensional massive fermionic system with parabolic bands [12,13], in contrast with the massless, conelike dispersion found in the monolayer. This limit is useful to compare the behavior of the bilayer (with its chirality) to that of the ordinary 2DEG, where experiments have shown that interactions play a dominant role, making the proper compressibility negative for small electron densities [14] as opposed to a positive constant given by the noninteracting model. This behavior is already present at the Hartree-Fock level. Because of the aforementioned mapping, *a priori*, it is reasonable to expect that the effect of electron-electron interactions would be observable in the graphene bilayer.

In this Letter, we calculate within the Hartree-Fock approximation the dependence of the inverse compressibility on the Fermi vector k_F using both a full, four-band ($4B$) model and the two-band ($2B$) approximation, which is valid for very small doping. We show that the most important qualitative signatures of the compressibility are already present at the $2B$ model level but that the $4B$ calculation, while more cumbersome, reveals finer features.

Throughout this Letter, we will refer (loosely) to the quantity $\tilde{\kappa}^{-1} = \partial\mu/\partial n_e$ as the "inverse compressibility." Here, μ stands for the chemical potential of the system. $\tilde{\kappa}$ differs by a factor of n_e^2 from κ in (1). This is appropriate since $\tilde{\kappa}^{-1}$ is usually the actual experimentally measured quantity. The density of electrons is given by $n_e = g_S g_v k_F^2/(4\pi)$, with $g_s = 2$, $g_v = 2$ being the spin and valley degeneracy, respectively. In the following, we will consider the case of small doping but outside the range of ferromagnetic instability that is found at extremely low doping [13]. At the Hartree-Fock level, the ground state energy is given by $E = K + E_{\text{ex}}$, where K stands for the kinetic energy and E_{ex} is the exchange energy per unit of area.

A graphene bilayer consists of two planes of graphene stacked as shown in Fig. 1. The kinetic term of the Hamiltonian can be written, in the nearest neighbor tight binding approximation [15], by expanding around the K, K' points of the Brillouin zone, as $\mathcal{H}_{\rm kin} = \sum_{\mathcal{Q}} \psi^\dagger_{\mathcal{Q}} \mathcal{K}(\mathbf{p}) \psi_{\mathcal{Q}}$ with $\psi^\dagger_{\mathcal{Q}} = (c^\dagger_{\mathbf{p},A_1,\sigma,a}, c^\dagger_{\mathbf{p},B_1,\sigma,a}, c^\dagger_{\mathbf{p},B_2,\sigma,a}, c^\dagger_{\mathbf{p},A_2,\sigma,a})$ where a labels the valley, σ the spin, and A_i, B_i denotes the sublattice in the plane $i = 1, 2$. $\sum_{\mathcal{Q}}$ represents the sum over all the indices. The kinetic energy matrix is given by (we use units such that $\hbar = 1$)

$$\mathcal{K}(\mathbf{p}) = \begin{pmatrix} 0 & p e^{i\phi(\mathbf{p})} & -t_\perp & 0 \\ p e^{-i\phi(\mathbf{p})} & 0 & 0 & 0 \\ -t_\perp & 0 & 0 & p e^{-i\phi(\mathbf{p})} \\ 0 & 0 & p e^{i\phi(\mathbf{p})} & 0 \end{pmatrix}, \tag{2}$$

where $\tan\phi(\mathbf{p}) = p_y/p_x$, $t_\perp = 0.35$ eV is the interlayer hopping energy, and we have set $v_F = 3ta/2$ ($\approx$6.6 eV Å) to unity (t is the intralayer hopping energy and a the in-plane carbon-carbon distance). The interaction is given by the 2D Fourier transform of the 3D Coulomb potential, which is $V_{ip}(\mathbf{k}) = \frac{2\pi e^2}{\epsilon_0}\frac{1}{k}$ for the interaction among electrons within the same plane and $V_{op}(\mathbf{k}) = \frac{2\pi e^2}{\epsilon_0}\frac{e^{-kd}}{k}$ otherwise, being $d \approx 3.35$ Å the interplane distance.

The kinetic energy matrix (2) can be diagonalized by a unitary transformation $S^\dagger(\mathbf{p})$. The resulting dispersion bands (see Fig. 1) are: $E_1(p) = -\tilde{t} + E(p)$, $E_2(p) = \tilde{t} - E(p)$, $E_3(p) = \tilde{t} + E(p)$, and $E_4(p) = -\tilde{t} - E(p)$; being $E(p) = \sqrt{\tilde{t}^2 + p^2}$ and $\tilde{t} = t_\perp/2$. It is convenient to work with the symmetric and antisymmetric combinations of the layer densities, $\rho_\pm = \rho_1 \pm \rho_2$, which can be expressed in the diagonal basis as $\rho_\alpha(\mathbf{q}) = \sum_{\mathbf{p}} \Phi^\dagger(\mathbf{p}+\mathbf{q}) \chi^\alpha(\mathbf{p}+\mathbf{q}, \mathbf{p}) \Phi(\mathbf{p})$ with $\Phi(\mathbf{p}) = S^\dagger(\mathbf{p})\psi(\mathbf{p})$ and $\alpha = \pm$. The 4×4 matrices χ^α contain the information of the overlap due to the change of basis. Then, the interaction Hamiltonian takes the form $\mathcal{H}_I = [1/(2A)] \sum_{\mathbf{q}\neq 0} \times \sum_\alpha \rho_\alpha(\mathbf{q}) V_\alpha(\mathbf{q}) \rho_\alpha(\mathbf{q})$, and the exchange energy per unit area A can be written in the continuum as

$$E_{\rm ex} = -g_s g_v \frac{1}{2} \int \frac{d^2\mathbf{p}}{(2\pi)^2} \times \frac{d^2\mathbf{q}}{(2\pi)^2} \sum_{\alpha,i,j} \chi^\alpha_{ij}(\mathbf{q},\mathbf{p}) \chi^\alpha_{ji}(\mathbf{p},\mathbf{q}) n_i(q) n_j(p) V_\alpha(\mathbf{q}-\mathbf{p}), \tag{3}$$

where $i, j = 1, \ldots 4$; $n_i(q) = \langle \Phi^\dagger_i(\mathbf{q}) \Phi_i(\mathbf{q}) \rangle$, and $V_\pm(\mathbf{k}) = \frac{1}{2}[V_{ip}(\mathbf{k}) \pm V_{op}(\mathbf{k})]$. The occupation factors are given by $n_1(q) = \Theta(k_F - q)$ [$n_1(q) = 0$], $n_2(q) = 1$ [$n_2(q) = 1 - \Theta(k_F - q)$], $n_3(q) = 0$, and $n_4(q) = 1$ in the case of electron [hole] doping. This model however requires a cutoff Λ of the order of the inverse of the lattice parameter.

Being simpler to work with, and widely used as a starting point for calculations in the graphene bilayer, we start our analysis with the approximate $2B$ model that can be constructed at low energies by performing degenerate perturbation theory [12,13]. This results in an effective kinetic Hamiltonian:

$$\mathcal{H}_{\rm kin} = \sum_{\mathcal{Q}} \frac{p^2}{2\tilde{t}} \tilde{\psi}^\dagger_{\mathcal{Q}} \begin{pmatrix} 0 & e^{-2i\phi(\mathbf{p})} \\ e^{2i\phi(\mathbf{p})} & 0 \end{pmatrix} \tilde{\psi}_{\mathcal{Q}}, \tag{4}$$

with $\tilde{\psi}^\dagger_{\mathcal{Q}} = (c^\dagger_{\mathbf{p},B_1,\sigma,a}, c^\dagger_{\mathbf{p},A_2,\sigma,a})$. The result of the approximation is an effective model with opposite parabolic dispersion bands of energy $E_a = p^2/(2\tilde{t})$, $E_b = -p^2/(2\tilde{t})$ as shown in Fig. 1. The effective kinetic energy per unit area then is given by $K = (k_F^4 - \Lambda^4)/(4\pi\tilde{t})$ giving a kinetic contribution to the inverse compressibility of $\tilde{\kappa}_K^{-1} = \pi/(2\tilde{t})$.

In this reduced Hilbert space, Eq. (3) is still valid, but this time the $\chi^\alpha(\mathbf{p},\mathbf{q})$ are 2×2 matrices. Combining all the contributions and reinserting the units, we find the total inverse compressibility $\tilde{\kappa}^{-1}$ in the $2B$ model to be given by the expression

$$\tilde{\kappa}^{-1} = \frac{v_F \hbar}{\Lambda} \left\{ \frac{\pi}{2\tilde{t}} - \frac{g}{4k_F} \int_0^\pi d\theta \int_0^1 p\,dp \frac{\partial}{\partial k_F} \times \left[\frac{k_F}{r(p,1,\theta)} [1 + \cos(2\theta) e^{-dk_F r(p,1,\theta)}] + \frac{1}{r(p,k_F,\theta)} [\pm 1 - \cos(2\theta) e^{-dr(p,k_F,\theta)}] \right] \right\}. \tag{5}$$

Here, we have defined $r(p,q,\theta) = \sqrt{p^2 + q^2 - 2pq\cos\theta}$, $\tilde{t}$, k_F, and $1/d$ are in units of Λ, and $g = e^2/(v_F \epsilon_0)$ is the graphene coupling strength. The $\pm$ indicates the expression for electrons (+) or holes (−). The differing term however is roughly a constant and can be neglected for small doping. Therefore, in what follows, we will use the results for electron doping.

Figure 2 shows a plot of (5) as a function of k_F for $\tilde{t}/\Lambda = 0.026$, and $d\Lambda = 3.7$ ($\Lambda = 1.06 \approx 1$ Å^{-1}). As can

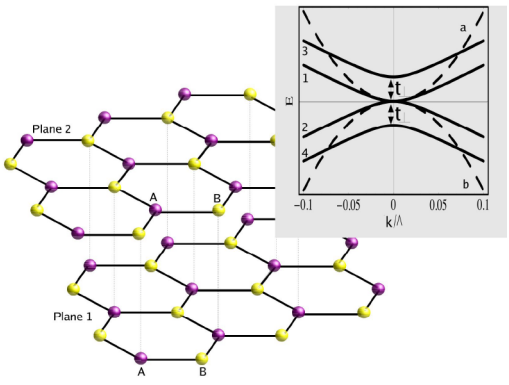

FIG. 1 (color online). Graphene bilayer lattice showing the two underlying sublattices A (dark) and B (light). *Inset*: $4B$ dispersion (continuous line) and $2B$ approximation (dashed line) as a function of momentum k. Momentum is in units of the cutoff Λ, measured from the K point.

be seen, for very small doping, the compressibility changes sign, becoming negative and divergent. This behavior, as mentioned previously, is also observed in the 2DEG. It is instructive to discriminate between inter and intraband contributions. Figure 2 also depicts the inverse compressibility when only the intraband transitions are considered (as well as the kinetic term, of course). From the difference with the curve for the total inverse compressibility, we can conclude that the interband contribution tends to move the negative region to smaller densities. The overall effect of the interband transitions then is to enhance $\tilde{\kappa}^{-1}$, therefore reducing the compressibility. This can be seen clearly from the inset in Fig. 2, where the contribution from intraband transitions is negative while that from interband transitions is positive. Apart from the sign, both present a similar behavior and are comparable in magnitude. In the $2B$ approximation, the kinetic contribution, as in the 2DEG case, is independent of the electronic density and is also plotted in Fig. 2 for reference. Therefore, the resulting total compressibility will be given by a competition of the two contributions. This difference in sign between inter and intraband contributions is analogous to the one present in monolayer graphene [8] and, within the $2B$ approximation, it can be interpreted in terms of the chirality of the quasiparticles. Intra (inter)-band exchange corresponds to interactions between particles of the same (opposite) chirality. Remarkably though, while for the monolayer the total exchange contribution is positive, for the bilayer, it is negative.

We can also compare with the usual result for the 2DEG. For this, we start from the expression for the chemical potential (see for example [16]) $\mu = \partial[n\epsilon(n)]/\partial n$, where $n = k_F^2/\pi$ is the electronic density (taking into account spin and valley degeneracy) and ϵ is the ground state energy per electron. If we consider only kinetic and exchange energy, $\epsilon = \epsilon_0 + \epsilon_{\mathrm{ex}}$ and for the 2DEG $\epsilon_0 = k_F^2/(4m)$, $\epsilon_{\mathrm{ex}} = -4e^2 k_F/(3\pi)$. Therefore, $\tilde{\kappa}^{-1}_{\mathrm{2DEG}} = (\pi/m - 2e^2/k_F)/2$. To compare with our case, we identify $\tilde{t} \equiv m$ and write $\tilde{\kappa}^{-1}_{\mathrm{2DEG}} = v_F/(2\Lambda)(\pi/\tilde{t} - 2g/k_F)$. The corresponding plot is also depicted in Fig. 2. Within the $2B$ approximation, the bilayer compressibility behaves qualitatively similar to that of the 2DEG, although because of the chiral nature of the bilayer system, the region of negative values is shifted to smaller values of the Fermi vector and therefore smaller densities.

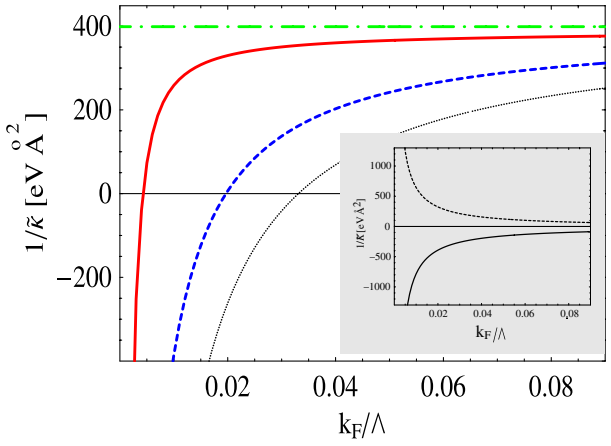

FIG. 2 (color online). Inverse compressibility vs Fermi wave vector in the 2-band approximation. Total: solid line, intraband plus kinetic contribution: dashed line, kinetic: dash/dot line, 2DEG: dotted line (black). The inset depicts the contribution of intraband exchange (solid line) and interband exchange (dashed line).

As mentioned above, the total compressibility of the bilayer is a product of the competition between inter and intraband contributions to exchange. However, from the inset in Fig. 2, it transpires that this is a very tight competition and small changes may alter the result. We therefore proceed to analyze the full $4B$ model. Because of the symmetries of the χ matrices, expression (3) is greatly simplified. The exchange contribution to the compressibility then is given by

$$\tilde{\kappa}^{-1}_{\mathrm{ex}} = -\frac{1}{8\pi k_F}\sum_{\alpha}\frac{\partial}{\partial k_F}(D^{\alpha}_{++} + D^{\alpha}_{+-})$$

being

$$D^{\alpha}_{++} = \int_0^{2\pi} d\theta \int_0^{k_F} p\,dp\,V_{\alpha}(|\mathbf{k}_F - \mathbf{p}|)|\chi^{\alpha}_{11}(\mathbf{k}_F, \mathbf{p})|^2,$$

$$D^{\alpha}_{+-} = \int_0^{2\pi} d\theta \int_0^{\Lambda} p\,dp\,V_{\alpha}(|\mathbf{k}_F - \mathbf{p}|)(|\chi^{\alpha}_{12}(\mathbf{k}_F, \mathbf{p})|^2 + |\chi^{\alpha}_{14}(\mathbf{k}_F, \mathbf{p})|^2),$$

where θ is the angle between $\mathbf{k}_F$, $\mathbf{p}$. As the notation suggests, D^{α}_{++} corresponds to exchange within the positive conduction band 1 while D^{α}_{+-} measures the exchange between the negative filled sea and the conduction band. The calculation for hole doping is completely analogous, with the overlap elements to be considered for that case being $|\chi^{\alpha}_{22}(\mathbf{k}_F, \mathbf{p})|^2$ and $|\chi^{\alpha}_{24}(\mathbf{k}_F, \mathbf{p})|^2$. Since the compressibility involves only occupied states, its behavior is not

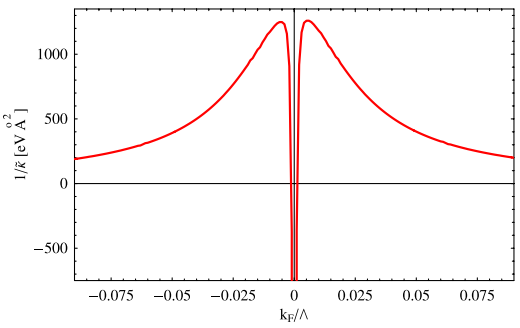

FIG. 3 (color online). Inverse compressibility as a function of the Fermi wave vector as calculated from the $4B$ model. Negative values of the Fermi vector indicate the result for hole doping.

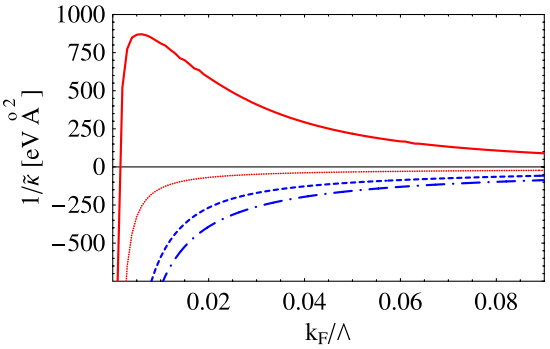

FIG. 4 (color online). Comparison between the exchange contribution for the $2B$ and $4B$ models. Total exchange: $4B$ solid line, $2B$ dotted line; intraband only: $4B$ dashed line, $2B$ dash/dot line.

symmetric with respect to particle-hole exchange. Nonetheless, the explicit calculation shows that the difference is negligible for small doping, being the same as in the $2B$ case. On the other hand, the kinetic contribution to the inverse compressibility is independent of the type of carrier, and it is easily calculated to be $\tilde{\kappa}_K^{-1} = \pi/[2E(p)]$. The final results for the four-band calculation, by summing all the contributions, is shown in Fig. 3.

We see that the full model confirms the major qualitative features found within the $2B$ approximation. The compressibility is negative for small electronic density, diverging in the limit of $k_F \to 0$, and the interband exchange contributes to the incompressibility of the system (see Fig. 4). The difference observed at larger values of the Fermi momentum is simply due to the difference in the kinetic term, since it is a constant in the two-band case while in the $4B$ model, it is $\sim 1/k_F$ for large k_F. However, a more detailed comparison reveals a peak in the inverse compressibility that is not captured in the $2B$ model. Overall, the $4B$ calculation predicts a more incompressible system in the range for which $\tilde{\kappa} > 0$, up to approximately 3 times larger than the prediction of the $2B$ model at the position of the peak. As seen from Fig. 4, the bulk of the difference between the $2B$ result and the $4B$ one comes from the interband exchange.

The $4B$ model seems to predict a behavior that is a hybrid between the one of a 2DEG, where the total contribution to the compressibility from exchange is negative, and the graphene monolayer, where it is positive.

In conclusion, we have studied the electronic compressibility of a graphene bilayer within the Hartree-Fock approximation and have found a behavior that is remarkably different from the two-dimensional electron gas due to the presence of interband transitions, and also from graphene monolayer. We have shown that the inverse compressibility is not a monotonic function of the electronic density and that the effective $2B$ model gives a good description of the problem only at very low densities. At intermediate densities, the four bands are important to explain the behavior of the compressibility. The nonmonotonic behavior of the compressibility obtained with the $4B$ model is highly unusual. Generally, nonmonotonicity is associated with some external factor, such as confinement or applied magnetic fields. However, here it is due solely to intrinsic electronic interactions. The implications of this remain to be understood. On the other hand, the negativity of the compressibility is understood once it is realized that the one involved is not the total compressibility but only that of the electronic gas. The total compressibility will comprise also the positive ionic background, which stabilizes the system. Nonetheless, the negative *divergence* of the inverse compressibility, present in both models for low enough electronic densities, could signal the eventual onset of Wigner crystallization [17]. These results, as in the case of the single layer graphene [8] can be studied via single electron transistor (SET) measurements. Our results indicate that the compressibility turns negative at density values of approximately $n_e \approx 10^{11}/\mathrm{cm}^2$, which borders the current available precision [8]. However, being a Hartree-Fock calculation, this can act just as a very rough estimate. We have also neglected the trigonal warping term, which might be of importance at very low densities [12].

We thank G. Giuliani, V. Kotov, B. Uchoa, G. Vignale, and A. Yacoby for illuminating discussions. S. V. K. would like to thank M. Reiris for his invaluable mathematical insight. A. H. C. N. was supported through NSF Grant No. DMR-0343790.

[1] See, A. K. Geim and K. S. Novoselov, Nat. Mater. **6**, 183 (2007), and references therein.
[2] A. H. Castro Neto, F. Guinea, and N. M. R. Peres, Phys. World **19**, 33 (2006).
[3] E. V. Castro *et al.*, arXiv:cond-mat/0611342.
[4] J. Nilsson and A. H. Castro Neto, Phys. Rev. Lett. **98**, 126801 (2007).
[5] T. Ohta *et al.*, Science **313**, 951 (2006).
[6] E. McCann, Phys. Rev. B **74**, 161403(R) (2006).
[7] K. S. Novoselov *et al.*, Nature Phys. **2**, 177 (2006).
[8] J. Martin *et al.*, arXiv:0705.2180.
[9] E. H. Hwang *et al.*, arXiv:cond-mat/0703499.
[10] Y. Barlas *et al.*, Phys. Rev. Lett. **98**, 236601 (2007).
[11] H. Suzuura and T. Ando, Phys. Rev. Lett. **89**, 266603 (2002).
[12] E. McCann and V. I. Fal'ko, Phys. Rev. Lett. **96**, 086805 (2006).
[13] J. Nilsson *et al.*, Phys. Rev. B **73**, 214418 (2006).
[14] J. P. Eisenstein, L. N. Pfeiffer, and K. W. West, Phys. Rev. B **50**, 1760 (1994).
[15] P. R. Wallace, Phys. Rev. **71**, 622 (1947).
[16] G. F. Giuliani and G. Vignale, *Quantum Theory of the Electron Liquid* (Cambridge University Press, Cambridge, England, 2005).
[17] H. P. Dahal *et al.*, arXiv:0706.1689v1.